Neuro-Oncology
27(4), 1116–1127, 2025 | https://doi.org/10.1093/neuonc/noae252 | Advance Access date 23 November 2024

Dynamic contrast-enhanced and diffusion-weighted MR imaging for predicting tumor growth of sporadic vestibular schwannomas: A prospective study

Sammy M. Schouten, Daniel Lewis, Stefan Cornelissen, Ka-Loh Li, Xiaoping Zhu, Marnix C. Maas, Sjoert Pegge, Thijs T.G. Jansen, Jef J.S. Mulder, Jérôme J. Waterval, Alida A. Postma, Omar Pathmanaban, David J. Coope, Jolanda M.M. Derks, Patrick P.J.H. Langenhuizen, Andrew T. King, Jeroen B. Verheul, Henricus P.M. Kunst

All author affiliations are listed at the end of the article

Corresponding Author: Sammy M. Schouten, MD, Department of Otolaryngology, Radboud University Medical Center, Geert Grooteplein Zuid 10, 6525 GA Nijmegen, the Netherlands (sammy.schouten@radboudumc.nl).

Abstract

Background. Advanced MR imaging, such as diffusion-weighted (DWI) and dynamic contrast-enhanced (DCE) imaging, may provide valuable noninvasive information on intrinsic tumor biology. This study aims to evaluate apparent diffusion coefficient (ADC) and DCE-MRI-derived microvascular parameter values (*Ktrans*, *ve*, and *vp*) as potential imaging predictors for future sporadic vestibular schwannoma (VS) growth.

Methods. In this prospective cohort study, patients with newly diagnosed unilateral sporadic VS and an initial wait-and-scan strategy were enrolled between January 2021 and January 2023. Patients underwent a single timepoint comprehensive MRI protocol, including DWI and DCE-MRI sequences. The estimated values of ADC, *Ktrans*, *ve*, and *vp* were calculated using established pipelines on a voxelwise basis within the delineated tumor region of interest. Associations of the estimated parameter values with volumetric growth were evaluated in uni- and multivariable logistic regression and survival analyses.

Results. Of the 110 analyzed patients, 70 (64%) exhibited growth during follow-up. A significant correlation was primarily observed between the DCE-MRI-derived parameters and VS growth. The combination of mean *Ktrans* ($P < .001$) and *ve* ($P < .001$) tumor values provided an internally validated model with an AUC of 0.85 for growth, yielding a sensitivity of 89% and specificity of 73% at the optimized cutoff value. Only the mean ADC values were found to be significantly higher in shrinking tumors ($P = .04$).

Conclusions. The strongly significant correlation observed between VS growth and *Ktrans* and *ve* tumor values indicate the great potential of the noninvasive DCE-MRI for individualized VS management in clinical practice. External validation is needed to further substantiate these findings.

Key Points

- Higher mean K^{trans} and lower mean v_e tumor values are strongly associated with VS growth.
- The use of K^{trans} and v_e tumor values may offer reliable, individualized predictions for VS growth.

Vestibular schwannomas (VS) are benign tumors arising from the eighth cranial nerve within the cerebellopontine angle (CPA), constituting approximately 8% of all primary intracranial tumors. The preferred initial management strategy for small- to medium-sized tumors is the conservative wait-and-scan (W&S) approach, since a substantial proportion of VS tumors remains stable or may even undergo regression following diagnosis, alongside the fact treatment does usually

Importance of the Study

The anticipation of growth serves as a pivotal consideration in clinical decision-making regarding sporadic vestibular schwannoma (VS). To date, there are still no reliable predictors for VS growth. Pilot studies suggest advanced MR imaging techniques, such as MR diffusion and dynamic contrast-enhanced (DCE) imaging, may offer valuable noninvasive information on intrinsic tumor biology. The findings from this prospective study reveal novel evidence regarding the use of these imaging biomarkers in predicting VS growth in clinical practice on an individual level. Results from this study demonstrate a strongly significant correlation between the DCE-MRI-derived K^{trans} and v_e tumor values and VS growth. The combination of these kinetic imaging parameters exhibits good to excellent discriminatory capacity between growing and nongrowing tumors. External validation is needed to further substantiate these findings.

not improve VS-related audio-vestibular symptoms.[1–5] When growth is observed, subsequent treatment with either stereotactic radiosurgery (SRS), microsurgery, or a combination of these methods may be pursued to prevent increased risk of mass effect complications of the neighboring neurovascular structures.[1,2]

The anticipated growth is therefore an essential factor in clinical decision-making for sporadic VS. Predicting VS growth on an individual basis would enable more careful monitoring and perhaps earlier intervention, resulting in improved patient counseling and optimized outcomes. Contrariwise, others can be monitored less strictly or may eventually be omitted from further follow-up. However, to date, there are still no reliable predictors for VS growth.[1]

Given the benign nature and intracranial location of VS, viable predictors in clinical practice are confined to noninvasive parameters, such as imaging. A growing body of pilot studies on advanced MR imaging techniques, such as MR diffusion-weighted imaging (DWI) and dynamic contrast-enhanced (DCE) imaging, have demonstrated promising potential to provide valuable noninvasive in vivo information on intrinsic VS tumor biology, using the specific derived biomarkers.[6–10]

Both imaging modalities can produce distinct tumor tissue characteristics. DCE imaging involves the evaluation of tissue microvascular features by acquiring imaging series postadministration of gadolinium-based contrast agents (GBCA).[11,12] Using model-based quantification, such as the extended Tofts model (ETM),[13] several key tissue microvascular kinetic parameters can be derived, including K^{trans}, v_e, and v_p. The volume transfer constant K^{trans}, the most widely used DCE-MRI-derived parameter, reflects the composite of tissue blood flow, vessel surface area, and vessel permeability. Whereas v_p and v_e represent the ratio of each image voxel occupied by blood plasma and extracellular extravascular space, respectively.[13] MR-DWI, on the other hand, involves evaluating tissue cellularity features by examining the random movement of water molecules within the tissue. This can be quantified using the apparent diffusion coefficient (ADC) value.[14]

The main aim of the present study is to prospectively assess the predictive value of ADC values and DCE-MRI-derived microvascular biomarkers in anticipating the short-term behavior of sporadic VS in clinical practice.

Methods

Study Population

Institutional review board approval was obtained by the regional medical ethics committee for this nonrandomized unblinded prospective study. Newly diagnosed patients with untreated unilateral sporadic VS subject for initial W&S approach were identified and approached via the Skull Base Unit at the Radboud University Medical Center Nijmegen between January 2021 and January 2023. The exclusion criteria were as follows: age under 18 years, NF2-related schwannomatosis (neurofibromatosis type 2), claustrophobia, contraindication to MRI scans or GBCA, ipsilateral cochlear implant to the VS or other implants causing imaging artifacts in the CPA region, and less than 1-year follow-up. Also, small intrameatal tumors under 6 mm maximum diameter were excluded due to decreased spatial resolution of the DWI and DCE-MRI to yield reliable ADC- and DCE-MRI-derived values. Written informed consent was obtained from all participants.

Baseline patient demographic data (age at the time of diagnosis, sex) and presenting symptomatology (hearing loss, tinnitus, vertigo, instability, facial paresis, and trigeminal dysfunction, including facial numbness or facial pain) were collected during the first hospital visit after diagnosis or referral. The hearing function was scored using the Gardner-Robertson hearing classification (GR).[15] The patient- and tumor characteristics are summarized with medians and interquartile ranges (IQRs) or with frequency counts and percentages.

MRI Acquisition and Imaging Timeline

Participants subsequently underwent a single timepoint comprehensive MRI study within 3 to 6 months following VS diagnosis on a 3T MAGNETOM Prismafit system using a 20-channel head and neck coil (Siemens Healthineers, Erlangen, Germany). The study MRI protocol included thin-slice 3-dimensional T2 weighted imaging, DWI, precontrast quantitative T1 mapping to determine native tissue T1 relaxation time prior to the arrival of contrast agent, and DCE imaging sequences (see Supplementary Methods). Following the study MRI scan, participants continued the usual standard-of-care follow-up regimen with conventional high-resolution T2-weighted sequences (for Koos

grade 1 & 2: 1, 2, 4, 7, and 10 years after diagnosis; for Koos grade 3 & 4: 1, 2, 4, 6, 8, and 10 years after diagnosis). When (continued) radiographic growth was observed during follow-up in extrameatal VS, participants converted to treatment according to the usual standard of care.

Image Analysis

Volumetric annotation.—Tumor volume measurements were manually performed slice-by-slice with ITK-SNAP software (version 3.8.0) on the high-resolution T2-weighted sequences.[16] Annotation was performed by the first author (S.M.S.). To enhance reliability of the measurements and reduce inter-observer variability, a second annotator (S.C) independently reviewed the annotations. Any necessary changes identified during this review process were resolved between the two authors. A previously published inter-observer variability study involving the same annotators yielded a mean inter-rater correlation coefficient of 0.99 for tumor volume segmentation, demonstrating excellent agreement between the annotators.[17]

The defined significant volumetric relative change threshold was tumor-volume dependent. The threshold was determined by using the subject-specific tumor volume at diagnosis to calculate the upper limit of agreement (LOAM) with the online calculator (https://vs-study.shinyapps.io/loamcalculation/) as proposed by Cornelissen et al.[17] The resulting thresholds range approximately from 5% to 30%, depending on the tumor size.

Tumor volumes during follow-up were subsequently assessed in relation to the volume at the time of diagnosis to identify growth or shrinkage. If growth or shrinkage was identified at the time of the study MRI scan, the event was considered significant when progression or regression persisted in the succeeding follow-up scan.

DCE-MRI & DWI analysis.—For vascular input function derivation, the middle cerebral artery and a previously described semiautomatic extraction method were used.[18,19]

Voxelwise signal intensity-time curves were converted to GBCA concentration–time curves using measured values of native tissue longitudinal relaxation rate ($R1_N$) derived from the precontrast T1 mapping series. GBCA concentration–time curves from each patient were then fitted to the ETM. As part of this fitting procedure, a map of scaled fitting error (SFE) was also generated to assess the discrepancy between the derived curve and the original data, and tumor voxels with an SFE value above 50% were excluded from the statistics.[20,21] The DCE-MRI analysis and map generation for all included tumors was conducted by analysts K.L., X.Z., and D.L. who were blinded to outcome growth. Further details on the DCE-MRI analysis and map generation are provided within the Supplementary Methods.

The ADC maps were calculated from native diffusion-weighted images on a voxelwise basis using the scanner software. The ADC values in the generated maps were similarly calculated on a voxelwise basis.

Delineation of tumor region of interest.—The volumetric tumor annotations, performed on the thin-slice 3-dimensional T2 weighted sequences of the study MRI scan, were used to determine the 3D tumor region of interest (ROI). Considering potential partial volume effects and the lower spatial resolution in DWI and DCE-MRI series, the ROI was fully contained within the tumor boundaries (see case example in Supplementary Figure S1). In tumors with cystic components, the delineation was manually adjusted to exclusively encompass the solid tumor region, given that cystic components lack cellularity and microvascularity. Subsequently, the eroded (adjusted) delineation was co-registered with the diffusion-weighted and DCE images separately to create an object mask per sequence type. The co-registered designated object mask was then projected onto the generated *ADC*, K^{trans}, v_e, and v_p maps to estimate the derived mean parameter values of the whole tumor. Data extraction was conducted by S.M.S., while remaining blinded to the outcome. Independent cross-verification was performed by S.C. to ensure the consistency and accuracy of the extracted data.

Statistical Analysis

Associations of mean *ADC*, K^{trans}, v_e, and v_p values within the tumor ROI with tumor growth were evaluated using uni- and multivariable logistic regression models and summarized with odds ratios and 95% confidence intervals. The tumor biomarker values were categorized into quartiles when a nonlinear association was found with the log odds probability for growth. The covariates age, tumor volume, presence of cystic components, and the mean beforementioned MRI parameter values were selected for multivariable analyses. A backward selection procedure was used until the model only contained variables with *P*-values of < .10. Models derived from multivariable regression analyses are known for overfitting. To avoid overfitting results, the resultant model was subsequently validated internally using bootstrapping techniques. Five hundred samples were drawn with replacements from the development sample. A shrinkage factor was generated to adjust the regression coefficients, and the offset procedure was used to generate a new intercept.[22] Thereafter, the final model performance was evaluated (see Supplementary Methods for further details). The discriminative ability of the model was assessed by the area under the receiver operating characteristic curve (AUC). Calibration was tested using the Hosmer–Lemeshow test; a *P*-value > .05 is regarded as a good model fit. Growth-free 1- and 2-year survival rates were estimated using the Kaplan–Meier method and the log-rank test for comparison. Follow-up duration was calculated from the date of VS diagnosis to the date of the last follow-up.

Values for $P < 0.05$ were considered significant. Statistical analyses were performed with SPSS Statistics for Windows, version 26 (IBM Corporation, Armonk, NY, USA). Internal validation procedures were performed with R for Windows, version 4.4.0 (R version 3.5.1 (R Foundation for Statistical Computing, Vienna, Austria)).

Results

Study Population and Parameter Values

Between January 2021 and January 2023, 118 participants were included in the study. Of these, 110 patients could be analyzed (Figure 1). The median age at diagnosis was 58

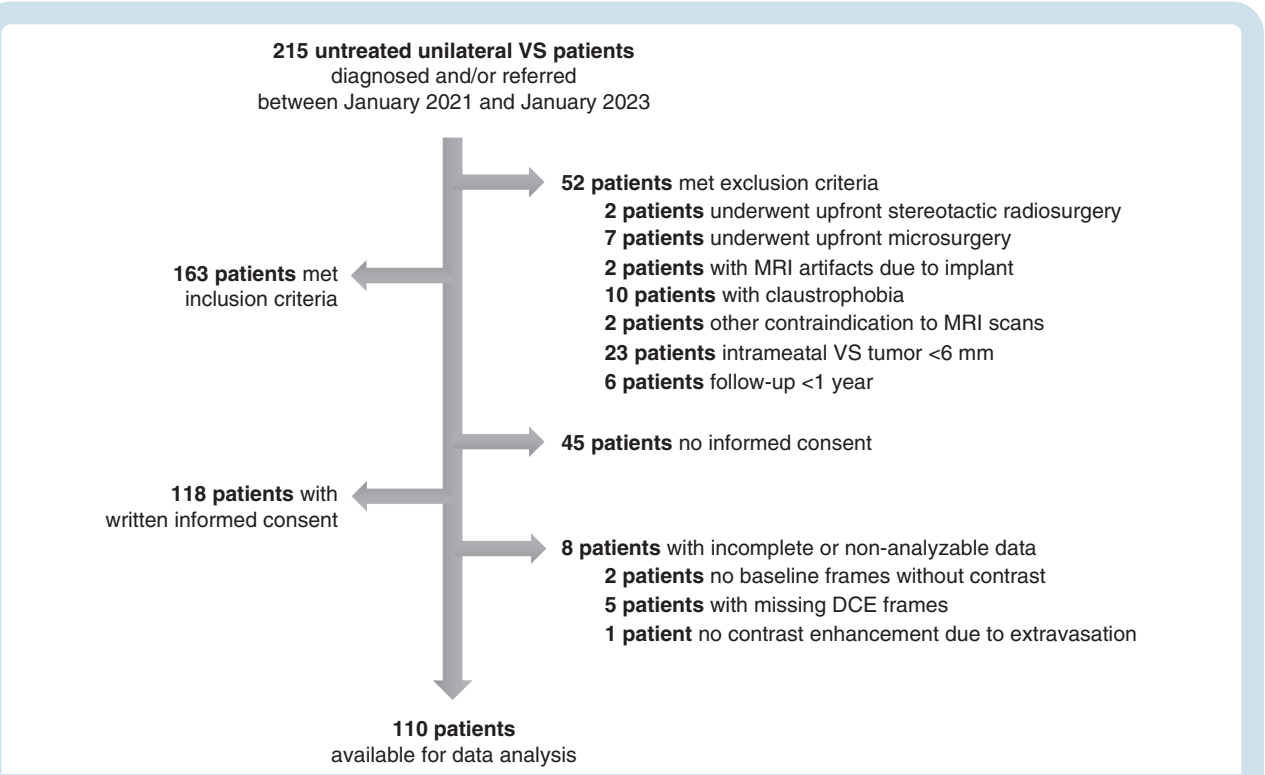

Figure 1. Flow diagram of the study population.

years old (IQR 48–67). Concerning the presenting symptomatology at diagnosis, 72 patients (65%) had serviceable hearing (GR1 & 2), and 10 patients (9%) suffered from trigeminal dysfunction. The median tumor size at diagnosis was 0.7 cm^3 (IQR 0.2–2.3), and 23 tumors (21%) had cystic components. The median tumor mean ADC values were 1288 * 10^{-6} mm^2/s (IQR 1113–1466). The median tumor mean K^{trans}, v_e, and v_p values were 0.10 min^{-1} (IQR 0.07–0.16), 0.35 (IQR 0.22–0.35), and 0.03 (IQR 0.02–0.06), respectively. Patient- and tumor characteristics are summarized in Table 1, and the imaging biomarker values are summarized in Figure 2.

Follow-up

Among the 110 tumors, growth, stability, and regression were observed in 70 (64%), 25 (23%), and 15 tumors (14%), respectively. Ultimately, 50 patients (45%) converted to active treatment during follow-up, all due to observed radiographic progression: 48 patients underwent primary SRS, and 2 patients underwent primary microsurgery. The median time to treatment was 15 months (IQR 9–22). The median time of follow-up among the patients with nongrowing tumors was 25 months (IQR 17–35).

Association between Tumor Imaging Biomarkers and Growth: Univariable Analysis

Univariable associations of the mean tumor biomarker values with tumor growth are presented in Table 2. Due to nonlinear associations with the log odds outcome growth, the biomarker tumor values were categorized into quartiles. In univariable analyses, K^{trans} ($P = .002$), v_e ($P = .007$), and v_p ($P = .02$) demonstrated significant associations with tumor growth. Mean K^{trans} values of 0.16 min^{-1} and above exhibited a significant OR of 15.6 for growth (95% CI, 3.8–65) compared to K^{trans} values of 0.07 min^{-1} and below. Mean v_e values below 0.27 showed a significant OR of 4.5 (95% CI, 1.3–16) for growth compared to values above 0.45. Only the fourth quartile of mean v_p values of 0.06 and above exhibited a significant OR of 3.9 for growth (95% CI, 1.1–14) compared to the first quartile of v_p values of 0.02 and below. The other quartiles did not significantly differ from one another. Mean ADC tumor values were not significantly associated with growth overall. However, in univariable ANOVA analyses mean ADC tumor values were significantly higher ($P = .04$) in shrinking tumors compared to the stable and growing tumors, with a mean difference of 262 * 10^{-6} mm^2/s (95% CI, 150–384) and 207 (95% CI, 101–321), respectively (Figure 2D).

Association between Tumor Imaging Biomarkers and Growth: Multivariable Analysis

In multivariable analyses following backward selection, only K^{trans} ($P < .001$) and v_e ($P < .001$) ended up as significant predictors for growth (Table 2). Internal validation on the resultant model was performed, and regression coefficients were adjusted with a shrinkage factor of 0.79. Discrimination of the final model yielded an AUC of 0.85 (95% CI, 0.77–0.93), indicating good to excellent

Table 1. Summary of Patient- and Tumor Characteristics and Follow-up[a]

Characteristic	Total $N = 110$
Age at diagnosis in years	58 (48-67)
Male gender	57 (52)
Gardner–Robertson scale	
1	31 (28)
2	41 (37)
3	28 (26)
4	5 (5)
5	5 (5)
Koos grade	
1	22 (20)
2	30 (27)
3	15 (14)
4	43 (39)
Tinnitus	85 (77)
Instability	45 (41)
Vertigo	9 (8)
Trigeminal dysfunction	10 (9)
Facial numbness	10 (9)
Facial pain	0 (0)
Facial paresis	0 (0)
Volume in cm^3	0.7 (0.2–2.3)
Maximum extrameatal diameter in mm[b]	13 (7–18)
Number of follow-up MRIs[c]	3 (2–4)
Cystic components	23 (21)
Microcystic	15 (14)
Macrocystic	8 (7)
Conversion to treatment	50 (45)
Stereotactic radiosurgery	48 (44)
Microsurgery	2 (2)
Microsurgery with adjuvant SRS	0 (0)
Time to treatment in months	15 (9–22)
Time to growth in months	10 (4–15)
Follow-up time in months of nongrowing tumors	25 (17–35)

Abbreviation: SRS = stereotactic radiosurgery.
[a]Summarized with median (IQR) or *n* (% of total).
[b]Maximum extrameatal diameter.
[c]Excluding diagnostic MRI.

performance. For calibration, the Hosmer–Lemeshow test yielded a statistic of 0.75, exceeding the significance threshold of 0.05, indicative of a well-fitted model. With the optimum cutoff value at 0.568, a sensitivity of 89%, specificity of 73%, PPV of 85%, and NPV of 78% were obtained (see Supplementary Methods). An online calculator (https://vs-mri-prediction.shinyapps.io/dce-mri/) was created to easily calculate the probability of VS growth. Furthermore, the interaction of size, age, and cystic components with the mean biomarker values was individually assessed, with none demonstrating significance for growth.

Growth-Free Survival Analyses

Growth-free survival rates (95% CI; numbers still at risk) at 1 and 2 years were 63% (58–68; 69) and 39% (34–44; 30), respectively (Figure 3A). Growth-free survival rates were significantly lower in tumors with higher mean K^{trans} values (chi-square = 16.3; *P*-value = .001) and in tumors with lower mean v_e values (chi-square = 15.1; *P*-value = .002) (Figure 3B and C). Growth-free survival rates at 1 and 2 years for tumors with a mean K^{trans} value of 0.16 and above, compared to tumors with values 0.07 and below, were 44% (34–54; 12), and 19% (10–26; 4), respectively, versus 82% (75–89; 22), and 74% (66–82; 15), respectively. Growth-free survival rates at 1 and 2 years for tumors with a mean v_e value below 0.27, compared to tumors with values above 0.45, were 67% (58–76; 18), and 18% (10–26; 3), respectively, versus 70% (61–79; 19), and 59% (50–69; 13), respectively.

Discussion

To our knowledge, this prospective study is the first to investigate the utilization of advanced MRI techniques and their derived parameters for predicting VS growth on a large clinical scale. In this study, our results demonstrate a strongly significant correlation between the DCE-MRI-derived microvascular kinetic parameters and short-term VS growth in logistic regression and survival analyses. Through multivariable logistic regression analyses, the combination of the mean K^{trans} ($P < .001$) and v_e ($P < .001$) tumor values provided an internally validated model with good to excellent discrimination (AUC 0.85) between the growing and nongrowing VS tumors, yielding a sensitivity of 89%, specificity of 73%, PPV of 85%, and NPV of 78%, at the optimized probability cutoff value of 0.568 (see Supplementary Methods and online probability calculator for VS growth: https://vs-mri-prediction.shinyapps.io/dce-mri/). This observed significant association with vascular permeability and growth is consistent with the findings of the pilot study conducted by Lewis et al.,[6] where growing VS tumors also exhibited significantly higher mean K^{trans} tumor values compared to the stable VS tumors. However, the particular correlation of lower mean v_e values with growing tumors has not been observed in these investigations. This discrepancy is likely attributed to the relatively smaller cohort sizes in previous studies. Notably, in other oncological investigations, correlations between mean v_e tumor values and tumor growth or tumor response to chemotherapy have been documented.[23–25]

Given that vestibular schwannomas are highly permeable, vascular tumors, the utilization of these DCE-MRI-derived microvascular metrics for assessing current tumor status is biologically plausible. Increasing evidence from ex vivo and in vivo studies suggests that inflammation may be critically important in driving tumor behavior.[6,26,27]

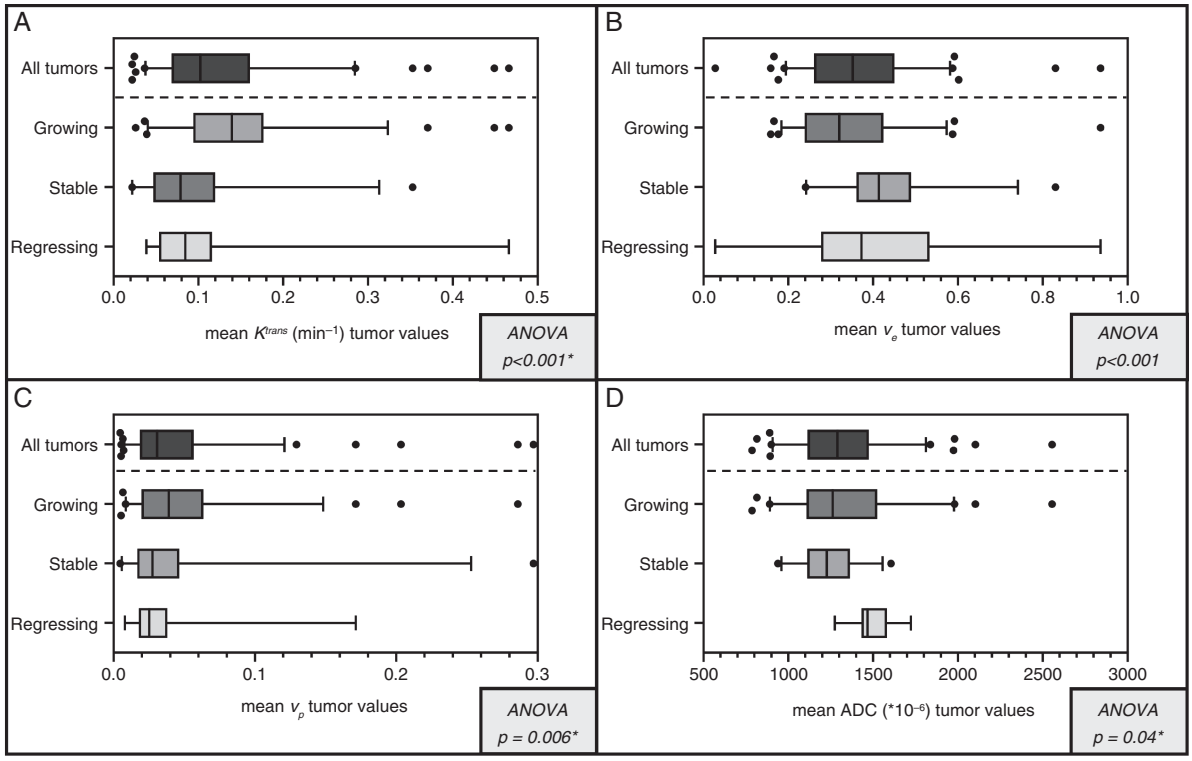

Figure 2. Summarizing boxplots with 5–95 percentile whiskers of mean (A) *K*trans, (B) v_e, (C) v_p, and (D) ADC tumor values of growing ($N = 70$), stable ($N = 25$) and regressing ($N = 15$) tumors. Comparison of growing, stable and regressing tumors using one-way ANOVA analysis. *Log-transformed due to right skewness.

Together with the emerging body of natural history evidence of stabilized indolent VS tumors that even tend to regress over time, it may be assumed that the tumor microenvironment of these nongrowing or static tumors has decreased activity, in terms of vascularity and flow, compared to actively growing VS. The principal DCE-MRI-derived parameter, K^{trans}, reflects the composite of tissue blood flow, vessel surface area, and vessel permeability. Consequently, higher blood flow and/or vessel permeability are reflected in higher K^{trans} values. Similarly, the parameter v_e represents the ratio of extracellular extravascular space within each image voxel, which can also be interpreted as the available "leakage space" within the tissue interstitium for GBCA accumulation. More "leakage space" within the tumor interstitium is reflected in higher v_e values. In the nongrowing tumors, we observed significantly lower mean K^{trans} values and higher v_e values compared to the actively growing tumors. Some evidence has shown that in growing VS, K^{trans} scales with tumor-associated macrophage (TAM) infiltration. One possible interpretation of high K^{trans} and low v_e in the most actively growing tumors is that the dense infiltration of macrophages reduces the EES by increasing the intracellular fraction, and once these tumors enter an indolent state, the intracellular fraction subsequently decreases.[28] Other vestibular schwannoma studies have observed a significant decrease in mean K^{trans} values over time in regressing and stable tumors following SRS, further supporting the hypothesis of decreased vascular permeability and flow in nongrowing tumors.[9,29]

Previous reports on the MRI-DWI have shown that pretreatment ADC values have potential in predicting VS tumor control post-SRS. ADC values quantify tissue cellularity features by examining the random movement of water molecules within the tissue. To our knowledge, the specific use of ADC values for predicting VS tumor growth has not been reported before. The mean ADC tumor values failed to distinguish growing tumors versus nongrowing tumors in our study. Only when comparing the mean ADC tumor values of the regressing tumors to the nonregressing tumors, ie, the growing and stable VS, a significant ($P = .04$) difference was observed (Figure 2).

Higher ADC values have been correlated with lower cellularity.[30] An intuitive hypothesis is that regressing tumors exhibit decreasing cellularity, which in turn results in higher ADC values compared to growing or stabilized tumors. With decreasing cellularity, one would also expect increases in the DCE-MRI-derived v_e values. However, the measurement of v_e is dependent on GBCA delivery. If vascularity is also reduced in stabilized and shrinking tumors, this may explain the observed discrepancies of high ADC versus low v_e values. Multivariable analyses could not be performed to further assess this correlation due to the small sample size of 15 patients with observed VS shrinkage. A larger cohort and longer follow-up are needed to evaluate the true potential of ADC tumor values in predicting tumor regression.

Table 2. Results of Uni- and Multivariable Analyses between Tumor Imaging Biomarkers and Growth

Features		Univariable		Multivariable[b]	
		OR (95% CI)	***P*-value**	**OR (95% CI)**	***P*-value**
Mean ADC[a]		Overall	.14		
	786–1113	(ref)	N/A		
	1115–1286	0.52 (0.16–1.69)	.28		
	1290–1467	0.27 (0.08–0.89)	.03		
	1481–2555	0.75 (0.22–2.6)	.65		
Mean K^{trans}(min^{-1})[a]		Overall	.002	Overall	<.001
	0.02–0.07	(ref)	N/A	(ref)	N/A
	0.07–0.10	3.20 (1.04–9.85)	.04	4.6 (0.96–22.0)	.06
	0.10–0.16	3.24 (1.09–9.67)	.035	14.2 (2.43–82.8)	.003
	0.16–0.47	15.6 (3.76–64.8)	<.001	180 (21–1543)	<.001
Mean v_e[a]		Overall	.007	Overall	<.001
	0.03–0.26	4.52 (1.32–15.5)	.02	70.0 (8.71–563)	<.001
	0.27–0.35	4.13 (1.28–13.4)	.02	21.6 (3.54–132)	<.001
	0.35–0.45	0.93 (0.32–2.69)	.90	1.93 (0.41–9.22)	.41
	0.46–0.94	(ref)	N/A	(ref)	N/A
Mean v_p[a]		Overall	.02		
	0.005–0.02	(ref)	N/A		
	0.02–0.03	0.63 (0.21–1.88)	.41		
	0.03–0.06	1.66 (0.54–5.08)	.38		
	0.06–0.30	3.93 (1.13–13.6)	.03		

Abbreviation: ADC = apparent diffusion coefficient.
[a]Categorized in quartiles due to a nonlinear relationship with the log odds outcome growth, range of values reported per quartile.
[b]For multivariable analyses backward selection was performed using the covariates age, size, presence of cystic components, mean ADC, mean K^{trans}, mean v_e, and mean v_p.

This study is subject to several limitations. Firstly, as a single-center study, the results are obtained under uniform conditions, using a single type of 3T MRI scanner and MRI acquisition protocol, followed by the same analysis pipeline for all subjects. Consequently, it remains unclear to what extent the results are reproducible under different circumstances. The DCE-derived values in this study are, however, comparable to those obtained in the much smaller pilot study conducted by Lewis et al.,[6] in which patients were not only scanned under a different field strength (1.5T Philips scanner) but also imaged using a different whole brain dual-injection, dual temporal resolution DCE-MRI acquisition protocol.[6,31] Secondly, the prospective nature of this study limited the follow-up duration, thereby presenting short-term outcome results for VS. Nevertheless, by employing a volumetric outcome definition, conducting high-quality MR scans, and including relatively larger VS (53% of tumors are either Koos grade 3 or 4), there is an increased sensitivity in detecting growth. Previous studies have observed that most (ranging from 75% to 91%) growth is observed within the first two years following diagnosis.[5,32,33] With a median follow-up of 25 months for the nongrowing tumors, the growth prevalence of 64% in this study aligns with findings from prior volumetric studies, with prevalence rates ranging from 42% to 79%.[5,32–38] Thirdly, the follow-up scan intervals were not prefixed in this study and varied according to different Koos grades due to standard care follow-up protocol differences. While this is likely a minor concern, longer follow-ups would provide clearer insights into its impact on the results. Lastly, it is important to note that mean biomarker tumor values were used in this study. However, notable variations in the standard deviation of these values were observed within tumors (Table 2). In some larger tumors, there was considerable heterogeneity in measured K^{trans} values across the tumor with certain tumor subregions exhibiting higher K^{trans} values compared to others. Determining whether these clustered regions with higher K^{trans} values possess specific predictive value for VS growth might be valuable. In an earlier, small tissue study of very large VS, considerable heterogeneity in TAM and CD31$^+$ vessel density was observed, with regions of both high and low vascularity and TAM infiltration, respectively. Elevated cellular proliferation rates within these intra-tumoral regions of high TAM density were also demonstrated, suggesting that growth occurs within these subregions of high vascularity and TAM infiltration within an individual tumor.[39] The incorporation of radiomics and artificial intelligence in a prediction

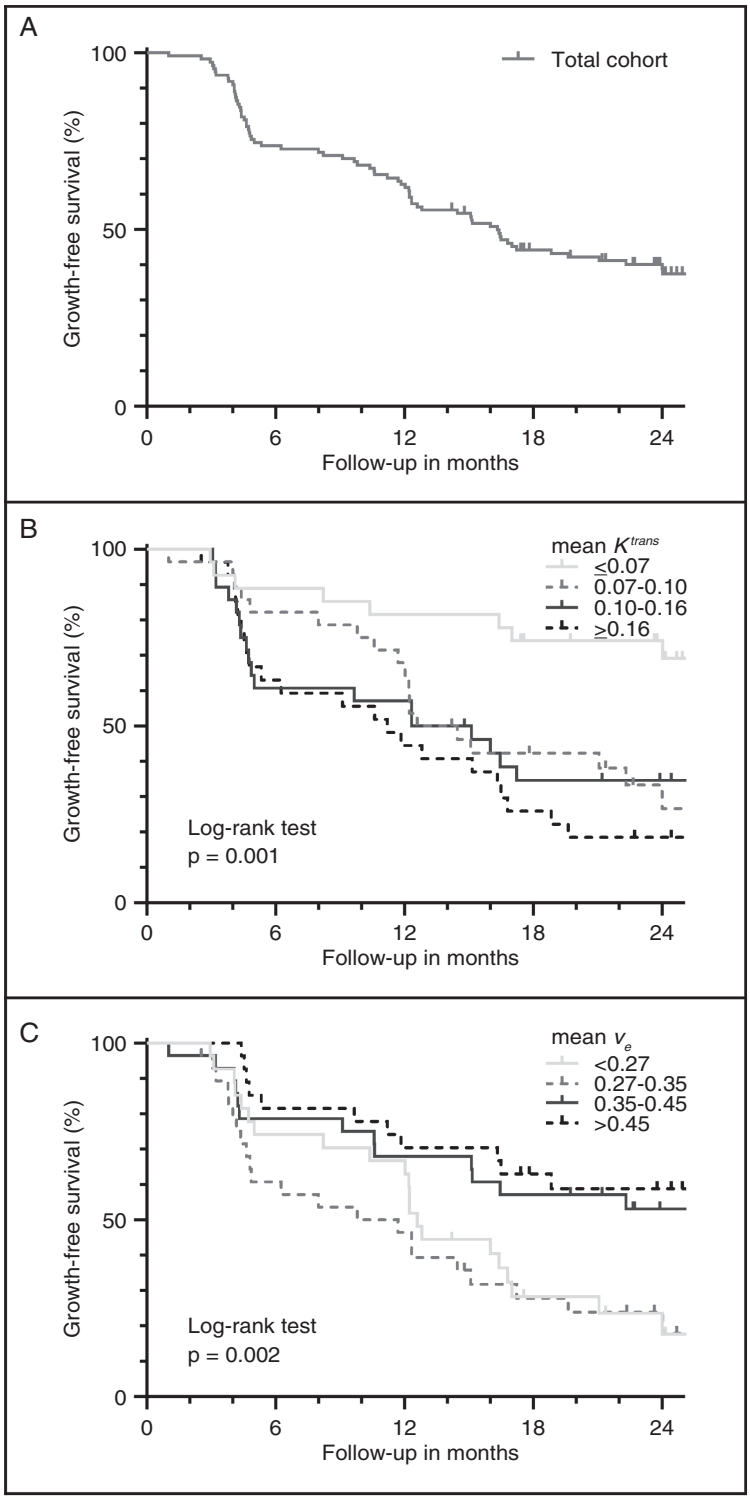

Figure 3. Kaplan–Meier survival curves of (A) growth-free survival rates of the total cohort; (B) growth-free survival rates stratified in mean *K*trans value quartiles; (C) growth-free survival rates stratified in mean v_e value quartiles.

model can potentially address these intra-tumoral value variations by using the generated DCE-derived maps as data input, presenting a promising direction for further research.

The utilization of ADC- and DCE-MRI-derived tumor values in clinical setting also entails specific challenges. One significant constraint is that these biomarker values are informative solely within the solid tumor component

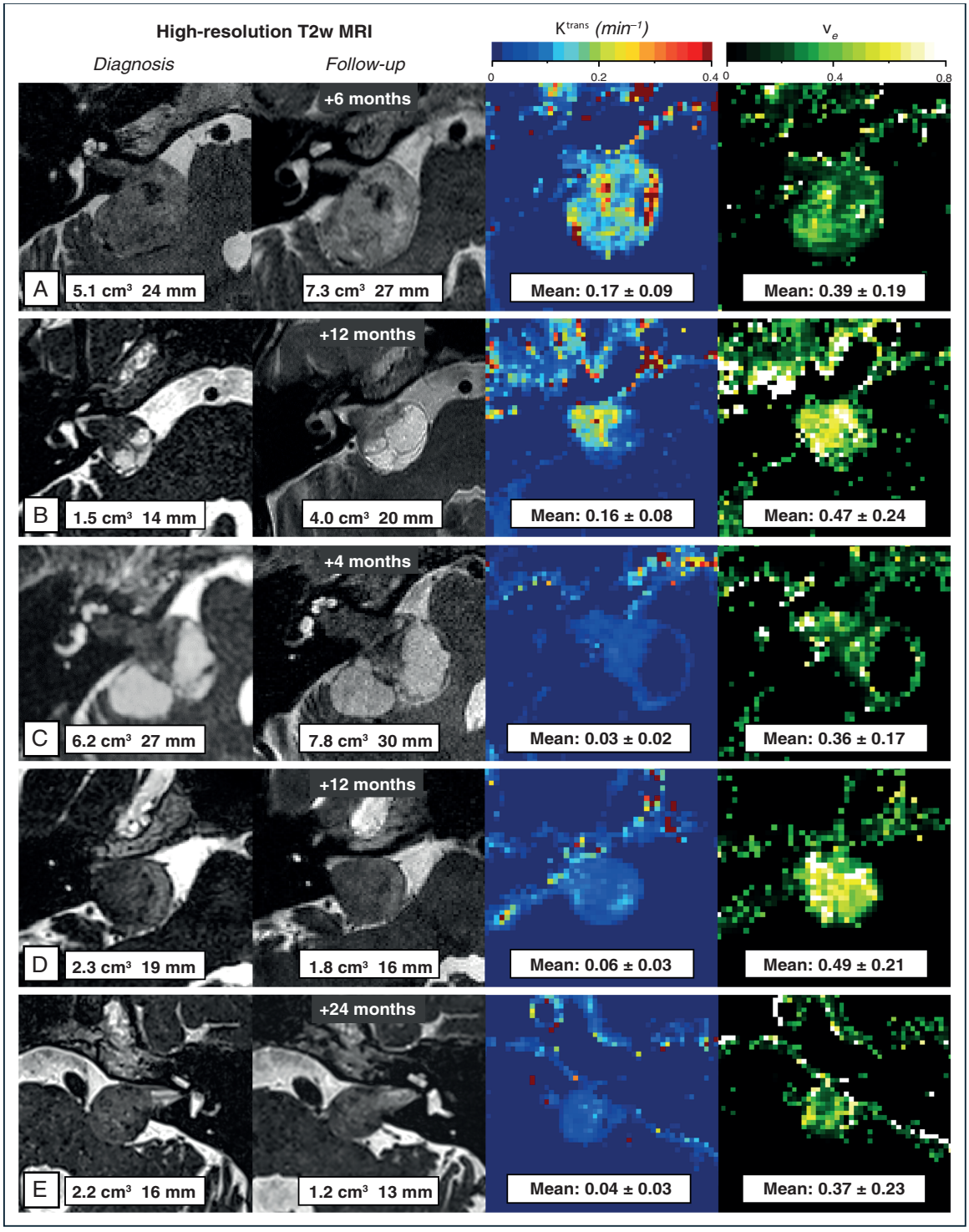

Figure 4. Case examples with size at diagnosis and at follow-up (volume in cm^3 and maximum extrameatal diameter in mm) with corresponding *K*trans and v_e (sfe50) maps: (A) growing tumor; (B) growing tumor with cystic components; (C) tumor with stable solid component, but growing cystic components; (D) regressing tumor; (E) regressing tumor.

and therefore do not offer dependable information on the cystic components. Although uncommon, existing literature acknowledges that solid and cystic components within the tumor can exhibit distinct behaviors.[5,40–43] In this study, one cystic tumor (Figure 4E) had a low mean K^{trans} value and a medium-high mean v_e value, thus a low risk for growth according to the model. While the solid components appeared stable during follow-up, the cystic components did

grow. In multivariable analyses, the interaction of cystic components with growth was additionally assessed for all parameters. It was found not to be significant, indicating that this case example is an outlier. Notwithstanding, it is still crucial to implement additional caution on a case-by-case basis with tumors containing peritumoral cystic components, despite a low risk for growth, ie, lower mean K^{trans} values and higher mean v^e values.

Another limitation concerning the extraction of ADC- and DCE-derived tumor values is observed in smaller tumor sizes. Due to the lower spatial resolution of the generated maps, dependable quantification of biomarker data confined solely within tumors smaller than 90 mm^3 could not be achieved. However, this constraint may be considered relatively minor, as the importance of growth prediction for these small intrameatal tumors is limited in a clinical setting. An increasing number of centers, including ours, adopt a strategy to continue surveillance despite tumor growth to a certain extrameatal threshold, before patients are converted to an active treatment strategy.[33,44–47] Therefore, predicting continued or rapid growth in these small intrameatal tumors would be more relevant, and it is still unknown whether the DCE-MRI-derived tumor values can provide this specific information due to the limited follow-up of this study.

Despite the acknowledged limitations and constraints, this prospective study offers novel insights into the use of noninvasive advanced MR techniques and their derived parameters for VS growth in clinical practice. The strongly significant correlation observed between tumor growth and the mean K^{trans} and v_e tumor values indicates great potential of the DCE-MRI within the work-up and management of VS on an individual level. The applicability and reproducibility should, however, be further explored through prospective multicenter external validation studies before the DCE-MRI can be implemented in other centers and integrated into clinical guidelines.

Supplementary material

Supplementary material is available online at *Neuro-Oncology* (https://academic.oup.com/neuro-oncology).

Keywords

advanced MRI | apparent diffusion coefficient | dynamic contrast-enhanced | vestibular schwannoma | volumetric growth

Funding

S.M.S., S.C., and P.P.J.H.L. are funded by the Highly Specialised Care & Research programme, (partly) financed by the Netherlands Organisation for Health Research and Development (ZonMw), Grant number 10070012010006. P.P.J.H.L. is also partly funded by Elekta AB, Stockholm, Sweden. D.L. is funded through a National Institute for Health Research (NIHR) Academic Clinical Lectureship at the University of Manchester, UK.

Conflict of interest statement

None declared.

Authorship statement

Experimental design and implementation: S.M.S., D.L., S.C., K.L, X.Z., M.C.M., S.P., T.T.G.J., J.J.S.M., J.J.W., A.A.P., O.P., D.J.C., J.M.M.D., P.P.J.H.L., A.T.K., J.B.V., H.P.M.K.; Image annotation: S.M.S.; Image analysis: S.M.S., D.L., K.L, X.Z.; Clinical data analysis and interpretation results: S.M.S., D.L., S.C., K.L, X.Z., J.M.M.D., P.P.J.H.L., J.B.V., H.P.M.K.; Manuscript writing and review and approval: S.M.S., D.L., S.C., K.L, X.Z., M.C.M., S.P., T.T.G.J., J.J.S.M., J.J.W., A.A.P., O.P., D.J.C., J.M.M.D., P.P.J.H.L., A.T.K., J.B.V., H.P.M.K.

Data availability

The data that support the findings of this study are not publicly available due to restrictions applying to the availability of these data. Data are, however, available from the corresponding author upon reasonable request and are located in controlled access data storage at the Radboud University Medical Center, Nijmegen, the Netherlands.

Previous presentations

A portion of this work has been presented at the Quadrennial VS Conference in May 2023 and at the ESBS Conference in June 2024 by S.M.S.

Affiliations

Radboud University Medical Center, Nijmegen, the Netherlands (S.M.S., M.C.M., S.P., T.T.G.J., J.J.S.M., J.M.M.D., H.P.M.K.); Maastricht University Medical Center+, Maastricht, the Netherlands (S.M.S., H.P.M.K., J.J.W., A.A.P.); Dutch Academic Alliance Skull Base Pathology Radboudumc/MUMC+, Nijmegen, the Netherlands (S.M.S., T.T.G.J., J.J.S.M., J.M.M.D., H.P.M.K., J.J.W., A.A.P.); Gamma Knife Center, Elisabeth-TweeSteden Hospital, Tilburg, the Netherlands (S.M.S., S.C., P.P.J.H.L., J.B.V.); Geoffrey Jefferson Brain Research Centre, University of Manchester, Manchester, UK (D.L., K.L., X.Z., O.P., D.J.C., A.T.K.); Division of Cancer Sciences, University of Manchester, Manchester, UK (D.L.); The Video Coding and Architecture Group, Eindhoven University of Technology, Eindhoven, the Netherlands (S.C., P.P.J.H.L.); Mental Health & Neuroscience

Research Institute, Maastricht University, Maastricht, the Netherlands (S.M.S., J.J.W., A.A.P., H.P.M.K.)

References

1. Carlson ML, Link MJ. Vestibular schwannomas. *N Engl J Med.* 2021;384(14):1335–1348.
2. Goldbrunner R, Weller M, Regis J, et al. Eano guideline on the diagnosis and treatment of vestibular schwannoma. *Neuro Oncol.* 2020;22(1):31–45.
3. Marinelli JP, Beeler CJ, Carlson ML, et al. Global incidence of sporadic vestibular schwannoma: A systematic review. *Otolaryngol Head Neck Surg.* 2022;167(2):209–214.
4. Reznitsky M, Petersen MMBS, West N, Stangerup SE, Cayé-Thomasen P. The natural history of vestibular schwannoma growth—prospective 40-year data from an unselected national cohort. *Neuro Oncol.* 2021;23(5):827–836.
5. Schouten SM, Cornelissen S, Langenhuizen PPHJ, et al. Wait-and-Scan management in sporadic Koos grade 4 vestibular schwannomas: A longitudinal volumetric study. *Neuro-Oncology Adv.* 2023;6(1):vdad144.
6. Lewis D, Roncaroli F, Agushi E, et al. Inflammation and vascular permeability correlate with growth in sporadic vestibular schwannoma. *Neuro Oncol.* 2019;21(3):314–325.
7. Camargo A, Schneider T, Liu L, et al. Pretreatment ADC values predict response to radiosurgery in vestibular schwannomas. *AJNR Am J Neuroradiol.* 2017;38(6):1200–1205.
8. Hwang I, Choi SH, Kim JW, et al. Response prediction of vestibular schwannoma after gamma-knife radiosurgery using pretreatment dynamic contrast-enhanced MRI: a prospective study. *Eur Radiol.* 2022;32(6):3734–3743.
9. Özer H, Yazol M, Erdoğan N, et al. Dynamic contrast-enhanced magnetic resonance imaging for evaluating early response to radiosurgery in patients with vestibular schwannoma. *Jpn J Radiol.* 2022;40(7):678–688.
10. Lewis D, Donofrio CA, O'Leary C, et al. The microenvironment in sporadic and neurofibromatosis type II–related vestibular schwannoma: the same tumor or different? A comparative imaging and neuropathology study. *J Neurosurg.* 2021;134(5):1419–1429.
11. Jackson A, Buckley DL, Parker GJM. *Dynamic Contrast-Enhanced Magnetic Resonance Imaging in Oncology.* Berlin, Heidelberg: Springer; 2005. doi:10.1007/b137553
12. O'Connor JPB, Jackson A, Parker GJM, Jayson GC. DCE-MRI biomarkers in the clinical evaluation of antiangiogenic and vascular disrupting agents. *Br J Cancer.* 2007;96(2):189–195.
13. Tofts PS, Brix G, Buckley DL, et al. Estimating kinetic parameters from dynamic contrast-enhanced T1- weighted MRI of a diffusable tracer: Standardized quantities and symbols. *J Magn Reson Imaging.* 1999;10(3):223–232.
14. Minati L, Węglarz WP. Physical foundations, models, and methods of diffusion magnetic resonance imaging of the brain: a review. *Concepts Magn Reson A.* 2007;30A(5):278–307.
15. Gardner G, Robertson JH. Hearing preservation in unilateral acoustic neuroma Surgery. *Ann Otol Rhinol Laryngol.* 1988;97(1):55–66.
16. Yushkevich PA, Piven J, Hazlett HC, et al. User-guided 3D active contour segmentation of anatomical structures: Significantly improved efficiency and reliability. *Neuroimage.* 2006;31(3):1116–1128.
17. Cornelissen S, Schouten SM, Langenhuizen PPJH, et al. Defining tumor growth in vestibular schwannomas: a volumetric inter-observer variability study in contrast-enhanced T1-weighted MRI. *Neuroradiology.* 2024;66(11):2033–2042.
18. Lewis D, Zhu X, Coope DJ, et al. Surrogate vascular input function measurements from the superior sagittal sinus are repeatable and provide tissue-validated kinetic parameters in brain DCE-MRI. *Sci Rep.* 2022;12(1):8737.
19. Zhu XP, Li KL, Kamaly-Asl ID, et al. Quantification of endothelial permeability, leakage space, and blood volume in brain tumors using combined T1 and T2* contrast-enhanced dynamic MR imaging. *J Magn Reson Imaging.* 2000;11(6):575–585.
20. Li K, Lewis D, Coope DJ, et al. The LEGATOS technique: A new tissue-validated dynamic contrast-enhanced MRI method for whole-brain, high-spatial resolution parametric mapping. *Magn Reson Med.* 2021;86(4):2122–2136.
21. Li K, Wilmes LJ, Henry RG, et al. Heterogeneity in the angiogenic response of a BT474 human breast cancer to a novel vascular endothelial growth factor-receptor tyrosine kinase inhibitor: Assessment by voxel analysis of dynamic contrast-enhanced MRI. *J Magn Reson Imaging.* 2005;22(4):511–519.
22. Moons KGM, Altman DG, Reitsma JB, et al. Transparent Reporting of a multivariable prediction model for Individual Prognosis Or Diagnosis (TRIPOD): Explanation and elaboration. *Ann Intern Med.* 2015;162(1):W1–73.
23. Lee J, Kim SH, Kang BJ. Pretreatment prediction of pathologic complete response to neoadjuvant chemotherapy in breast cancer: Perfusion metrics of dynamic contrast enhanced MRI. *Sci Rep.* 2018;8(1):1–8.
24. Park JJ, Kim CK, Park SY, et al. Assessment of early response to concurrent chemoradiotherapy in cervical cancer: Value of diffusion-weighted and dynamic contrast-enhanced MR imaging. *Magn Reson Imaging.* 2014;32(8):993–1000.
25. Chen Y, Yang X, Wen Z, et al. Association between high-resolution MRI-detected extramural vascular invasion and tumour microcirculation estimated by dynamic contrast-enhanced MRI in rectal cancer: Preliminary results. *BMC Cancer.* 2019;19(1):1–11.
26. Hannan CJ, Lewis D, O'Leary C, et al. The inflammatory microenvironment in vestibular schwannoma. *Neuro-Oncology Adv.* 2020;2(1):vdaa023.
27. Hannan CJ, Lewis D, O'Leary C, et al. Increased circulating chemokines and macrophage recruitment in growing vestibular schwannomas. *Neurosurgery.* 2023;92(3):581–589.
28. Committee. D. C. E. M. R. I. T. DCE MRI quantification profile, quantitative imaging biomarkers alliance. *Radiol Soc North Am.* 2012.
29. Lewis D, McHugh DJ, Li KL, et al. Detection of early changes in the post-radiosurgery vestibular schwannoma microenvironment using multinuclear MRI. *Sci Rep.* 2021;11(1):15712.
30. Harkins KD, Galons JP, Secomb TW, Trouard TP. Assessment of the effects of cellular tissue properties on ADC measurements by numerical simulation of water diffusion. *Magn Reson Med.* 2009;62(6):1414–1422.
31. Li KL, Buonaccorsi G, Thompson G, et al. An improved coverage and spatial resolutiona-using dual injection dynamic contrast-enhanced (ICE-DICE) MRI: A novel dynamic contrast-enhanced technique for cerebral tumors. *Magn Reson Med.* 2012;68(2):452–462.
32. Lees KA, Tombers NM, Link MJ, et al. Natural history of sporadic vestibular schwannoma: A volumetric study of tumor growth. *Otolaryngol Head Neck Surg.* 2018;159(3):535–542.
33. Marinelli JP, Schnurman Z, Killeen DE, et al. Long-term natural history and patterns of sporadic vestibular schwannoma growth: A multi-institutional volumetric analysis of 952 patients. *Neuro Oncol.* 2022;24(8):1298–1306.
34. Selleck AM, Rodriguez JD, Brown KD. Vestibular schwannoma measurements – Is volumetric analysis clinically necessary? *Otol Neurotol.* 2021;42(6):906–911.

35. Tomita Y, Tosaka M, Aihara M, Horiguchi K, Yoshimoto Y. Growth of primary and remnant vestibular schwannomas: A three-year follow-up study. *World Neurosurg.* 2015;83(6):937–944.
36. Varughese JK, Breivik CN, Wentzel-Larsen T, Lund-Johansen M. Growth of untreated vestibular schwannoma: A prospective study – Clinical article. *J Neurosurg.* 2012;116(4):706–712.
37. Van De Langenberg R, De Bondt BJ, Nelemans PJ, et al. Predictors of volumetric growth and auditory deterioration in vestibular schwannomas followed in a wait and scan policy. *Otol Neurotol.* 2011;32(2):338–344.
38. Caye-Thomasen P, Hansen S, Dethloff T, Stangerup SE, Thomsen J. Sublocalization and volumetric growth pattern of intracanalicular vestibular schwannomas. *Laryngoscope.* 2006;116(7):1131–1135.
39. Lewis D, Donofrio CA, O'Leary C, et al. The microenvironment in sporadic and neurofibromatosis type II-related vestibular schwannoma: the same tumor or different? A comparative imaging and neuropathology study. *J Neurosurg.* 2020;134(5):1419–1429.
40. Massaad E, Hamidi N, Goetz J, et al. Equivalent efficacy and safety of radiosurgery for cystic and solid vestibular schwannomas: A systematic review. *World Neurosurg.* 2021;146:322–331.e1.
41. Charabi S, Klinken L, Tos M, Thomsen J. Histopathology and growth pattern of cystic acoustic neuromas. *Laryngoscope.* 1994;104(11 Pt 1):1348–1352.
42. Charabi S, Mantoni M, Tos M, Thomsen J. Cystic vestibular schwannomas: Neuroimaging and growth rate. *J Laryngol Otol.* 1994;108(5):375–379.
43. Ali NES, Sayyid ZN, Alyono JC. Natural history of cystic vestibular schwannomas. *Ann Otol Rhinol Laryngol.* 2023;132(7):795–799.
44. Donghun K, Crowther JA, Taylor WAS, Locke R, Kontorinis G. How many growing vestibular schwannomas tend to stop growing without any treatment? *J Laryngol Otol.* 2023;137(2):127–132.
45. Jia H, Sterkers O, Pavillon-Maisonnier C, et al. Management and outcomes of sporadic vestibular schwannoma: A longitudinal study over 12 years. *Laryngoscope.* 2021;131(3):E970–E976.
46. Marinelli JP, Lohse CM, Carlson ML. Introducing an evidence-based approach to wait-and-scan management of sporadic vestibular schwannoma. *Otolaryngol Clin North Am.* 2023;56(3):445–457.
47. Macielak RJ, Wallerius KP, Lawlor SK, et al. Defining clinically significant tumor size in vestibular schwannoma to inform timing of microsurgery during wait-and-scan management: moving beyond minimum detectable growth. *J Neurosurg.* 2021;136(5):1289–1297.